PNAS RESEARCH ARTICLE | EARTH, ATMOSPHERIC, AND PLANETARY SCIENCES

Balance and imbalance in biogeochemical cycles reflect the operation of closed, exchange, and open sets

Preston Cosslett Kemeny[a,1], Mark A. Torres[b], Woodward W. Fischer[c], and Clara L. Blättler[a]

Edited by Donald Canfield, Syddansk Universitet, Odense, Denmark; received September 22, 2023; accepted February 9, 2024

Biogeochemical reactions modulate the chemical composition of the oceans and atmosphere, providing feedbacks that sustain planetary habitability over geological time. Here, we mathematically evaluate a suite of biogeochemical processes to identify combinations of reactions that stabilize atmospheric carbon dioxide by balancing fluxes of chemical species among the ocean, atmosphere, and geosphere. Unlike prior modeling efforts, this approach does not prescribe functional relationships between the rates of biogeochemical processes and environmental conditions. Our agnostic framework generates three types of stable reaction combinations: closed sets, where sources and sinks mutually cancel for all chemical reservoirs; exchange sets, where constant ocean–atmosphere conditions are maintained through the growth or destruction of crustal reservoirs; and open sets, where balance in alkalinity and carbon fluxes is accommodated by changes in other chemical components of seawater or the atmosphere. These three modes of operation have different characteristic timescales and may leave distinct evidence in the rock record. To provide a practical example of this theoretical framework, we applied the model to recast existing hypotheses for Cenozoic climate change based on feedbacks or shared forcing mechanisms. Overall, this work provides a systematic and simplified conceptual framework for understanding the function and evolution of global biogeochemical cycles.

element cycles | habitability | Earth history | seawater chemistry

Significance

Models of global element cycles seek to understand how biogeochemical processes and environmental conditions interact to sustain planetary habitability. However, outcomes from such models often reflect specific interpretations of geochemical archives. In this work, we perform a different type of calculation that identifies fundamental modes of biogeochemical variability. By remaining agnostic to the relationships between environmental conditions and the intensity of biogeochemical processes, our analysis recognizes and systematizes patterns that underly the stability of major element cycles. We demonstrate the utility of this framework by applying it to examine and synthesize existing hypotheses for climate change over the last 65 million years.

1. Biogeochemistry and habitability

The partial pressure of carbon dioxide in Earth's atmosphere (pCO_2) is among the most important drivers of Earth's climate. Despite evidence for its long-term stability (1), theory suggests that pCO_2 is extremely sensitive to even small imbalances between the input and output fluxes of carbon and alkalinity (ALK) to the ocean–atmosphere system (2, 3). To avoid unrealistic variations in pCO_2, numerical models of the long-term carbon cycle often employ a climate-dependent silicate weathering feedback that couples ALK production to environmental conditions (4). Although the hypothesis of a silicate weathering feedback is well founded (5), alternative or compensatory biogeochemical mechanisms for the regulation of atmospheric CO_2 have also been proposed and may be similarly important; these mechanisms stress the role of tectonics and erosion in promoting silicate weathering (6–8), organic carbon oxidation and burial (9–12), sulfuric acid production (13, 14), carbonate weathering and precipitation (15), and clay formation (16–18). Understanding the sets of biogeochemical reactions that can stabilize pCO_2, as well as how those processes impact the composition and size of Earth's crustal reservoirs, the major ion chemistry of seawater, and the redox state of the atmosphere, remain major challenges for understanding planetary habitability over geological timescales.

The output of long-term carbon cycle models can depend critically on the parameterizations that couple element fluxes to climate state or reflect specific interpretations of chemical archives. For example, models reflecting different perspectives on the $^{87}Sr/^{86}Sr$ record have elicited conflicting interpretations of reduced mafic weathering (19) or increased mafic weathering (20) throughout the Neogene. Moreover, even within the same numerical framework, changes in process equations or forcings can substantially alter model results (21–24). In contrast, here, we take a different, agnostic approach that avoids prescribing functional relationships between climate conditions and chemical fluxes. Our goal in this work is not to prescribe how biogeochemical processes relate to one another through possible shared dependencies, as that effort has occupied low-temperature geochemical box modeling for much of the preceding decades, but instead to provide a biogeochemical abstraction—a way to organize processes and fluxes without explicitly representing the evolution of Earth's reservoirs through time. Rather than constructing a time-evolving box model, here we instead consider a core set of biogeochemical processes and quantify their collective impacts on global element cycles. By evaluating inputs and outputs to the fluid Earth without enforcing subjective parameterizations for how those fluxes arise from

Author affiliations: [a]Department of the Geophysical Sciences, The University of Chicago, Chicago, IL; [b]Department of Earth, Environmental, and Planetary Sciences, Rice University, Houston, TX; and [c]Division of Geological and Planetary Sciences, California Institute of Technology, Pasadena, CA

Author contributions: P.C.K. designed research; P.C.K. performed research; P.C.K., M.A.T, W.W.F., and C.L.B. analyzed data; M.A.T., W.W.F., and C.L.B. advised on project; P.C.K. wrote the first draft of the paper, while M.A.T., W.W.F., and C.L.B. helped with review and editing of the manuscript; and P.C.K., M.A.T., W.W.F., and C.L.B. wrote the paper.

The authors declare no competing interest.

This article is a PNAS Direct Submission.

[1]To whom correspondence may be addressed. Email: preston.kemeny@gmail.com.

This article contains supporting information online at https://www.pnas.org/lookup/suppl/doi:10.1073/pnas.2316535121/-/DCSupplemental.

Published March 13, 2024.

Table 1. Biogeochemical reactions

#	Biogeochemical reaction	Chemical expression
1	Mantle degassing of CO_2	$CO_{2\,(mantle)} \rightarrow CO_2$
2	Mantle degassing of HCl	$HCl_{\,(mantle)} \rightarrow H^+ + Cl^-$
3	Mantle degassing of H_2S	$H_2S_{\,(mantle)} \rightarrow H_2S$
4	Calcite metamorphism	$CaCO_3 + SiO_{2\,(solid)} \rightarrow CO_2 + CaSiO_3$
5	Dolomite metamorphism	$CaMg(CO_3)_2 + 2SiO_{2\,(solid)} \rightarrow CaSiO_3 + MgSiO_3 + 2CO_2$
6	Siderite metamorphism	$FeCO_3 + SiO_{2\,(solid)} \rightarrow CO_2 + FeSiO_3$
7	Ca-silicate weathering	$2H^+ + CaSiO_3 \rightarrow Ca^{2+} + H_2O + SiO_{2\,(aq)}$
8	Mg-silicate weathering	$2H^+ + MgSiO_3 \rightarrow Mg^{2+} + H_2O + SiO_{2\,(aq)}$
9	Na-silicate weathering	$2H^+ + Na_2SiO_3 \rightarrow 2Na^+ + H_2O + SiO_{2\,(aq)}$
10	K-silicate weathering	$2H^+ + K_2SiO_3 \rightarrow 2K^+ + H_2O + SiO_{2\,(aq)}$
11	Fe-silicate weathering	$2H^+ + FeSiO_3 \rightarrow Fe^{2+} + H_2O + SiO_{2\,(aq)}$
12	Calcite weathering	$2H^+ + CaCO_3 \rightarrow Ca^{2+} + CO_2 + H_2O$
13	Dolomite weathering	$4H^+ + CaMg(CO_3)_2 \rightarrow Ca^{2+} + Mg^{2+} + 2CO_2 + 2H_2O$
14	Siderite weathering	$2H^+ + FeCO_3 \rightarrow Fe^{2+} + CO_2 + H_2O$
15	Silica weathering	$SiO_{2\,(solid)} \rightarrow SiO_{2\,(aq)}$
16	Mg-reverse weathering	$Mg^{2+} + H_2O + SiO_{2\,(aq)} \rightarrow 2H^+ + MgSiO_3$
17	Na-reverse weathering	$2Na^+ + H_2O + SiO_{2\,(aq)} \rightarrow 2H^+ + Na_2SiO_3$
18	K-reverse weathering	$2K^+ + H_2O + SiO_{2\,(aq)} \rightarrow 2H^+ + K_2SiO_3$
19	Fe-reverse weathering	$Fe^{2+} + H_2O + SiO_{2\,(aq)} \rightarrow 2H^+ + FeSiO_3$
20	Silica formation	$SiO_{2\,(aq)} \rightarrow SiO_{2\,(solid)}$
21	Calcite formation	$CO_2 + H_2O + Ca^{2+} \rightarrow 2H^+ + CaCO_3$
22	Dolomite formation	$2CO_2 + 2H_2O + Ca^{2+} + Mg^{2+} \rightarrow 4H^+ + CaMg(CO_3)_2$
23	Siderite formation	$CO_2 + H_2O + Fe^{2+} \rightarrow 2H^+ + FeCO_3$
24	Oxygenic photosynthesis	$CO_2 + H_2O \rightarrow CH_2O + O_2$
25	Aerobic respiration	$CH_2O + O_2 \rightarrow CO_2 + H_2O$
26	Sulfide oxidation	$H_2S + 2O_2 \rightarrow SO_4^{2-} + 2H^+$
27	Sulfate reduction	$2H^+ + SO_4^{2-} + 2CH_2O \rightarrow H_2S + 2CO_2 + 2H_2O$
28	Ferrous iron oxidation	$4Fe^{2+} + O_2 + 4H_2O \rightarrow 2Fe_2O_3 + 8H^+$
29	Ferric iron reduction	$8H^+ + 2Fe_2O_3 + CH_2O \rightarrow 4Fe^{2+} + CO_2 + 5H_2O$
30	Pyrite oxidation	$4FeS_2 + 15O_2 + 8H_2O \rightarrow 8SO_4^{2-} + 2Fe_2O_3 + 16H^+$
31	Pyrite formation	$2H_2S + Fe_2O_3 + 2H^+ \rightarrow FeS_2 + Fe^{2+} + 3H_2O$
32	Gypsum dissolution	$CaSO_4 \cdot 2H_2O \rightarrow Ca^{2+} + SO_4^{2-} + 2H_2O$
33	Gypsum formation	$Ca^{2+} + SO_4^{2-} + 2H_2O \rightarrow CaSO_4 \cdot 2H_2O$
34	Halite dissolution	$NaCl \rightarrow Na^+ + Cl^-$
35	Halite formation	$Na^+ + Cl^- \rightarrow NaCl$
36	Nitrogen fixation	$2N_2 + 6H_2O + 4H^+ \rightarrow 4NH_4^+ + 3O_2$
37	Nitrification	$NH_4^+ + 2O_2 \rightarrow NO_3^- + H_2O + 2H^+$
38	Denitrification	$4NO_3^- + 4H^+ + 5CH_2O \rightarrow 2N_2 + 7H_2O + 5CO_2$

Reactions describe mantle inputs (#1 to 3), metamorphism (#4 to 6), silicate weathering (#7 to 11), carbonate weathering (#12 to 14), silica weathering (#15), reverse weathering (#16 to 19), silica formation (#20), carbonate formation (#21 to 23), photosynthesis and aerobic respiration (#24 and 25), the cycling of sulfur and iron (#26 to 31), salt formation and dissolution (#32 to 35), and nitrogen cycling (#36 to 38). Solid compositions are idealized and specific environmental contexts are not considered. Each reaction runs unidirectionally to the right.

environmental conditions, we calculate the fundamental modes of carbon cycle stability. Although this work thus differs substantially from prior geochemical modeling efforts, it is necessarily informed by the history of box modeling (21, 25–30). Our approach parallels and extends that of Garrels and Perry (31); we first consider steady-state conditions for all chemical reservoirs, then evaluate how reactions can exchange mass among crustal reservoirs without altering ocean–atmosphere conditions, and finally consider how changes in the chemistry of the atmosphere and ocean can stabilize pCO_2. By formalizing how combinations of biogeochemical reactions impact element cycles, this work provides a systematic and simplified framework for understanding stability and instability in the biogeochemical components of Earth's climate over geological timescales.

2. Biogeochemical Reactions and Set Calculations

Our analysis is built from a suite of biogeochemical processes that influence the chemical composition of the fluid Earth (Table 1). These processes include mantle degassing of CO_2, hydrochloric acid (HCl), and hydrogen sulfide (H_2S); metamorphism and precipitation of calcite, dolomite, and siderite; weathering and reverse weathering (authigenic silicate mineral formation) of calcium,

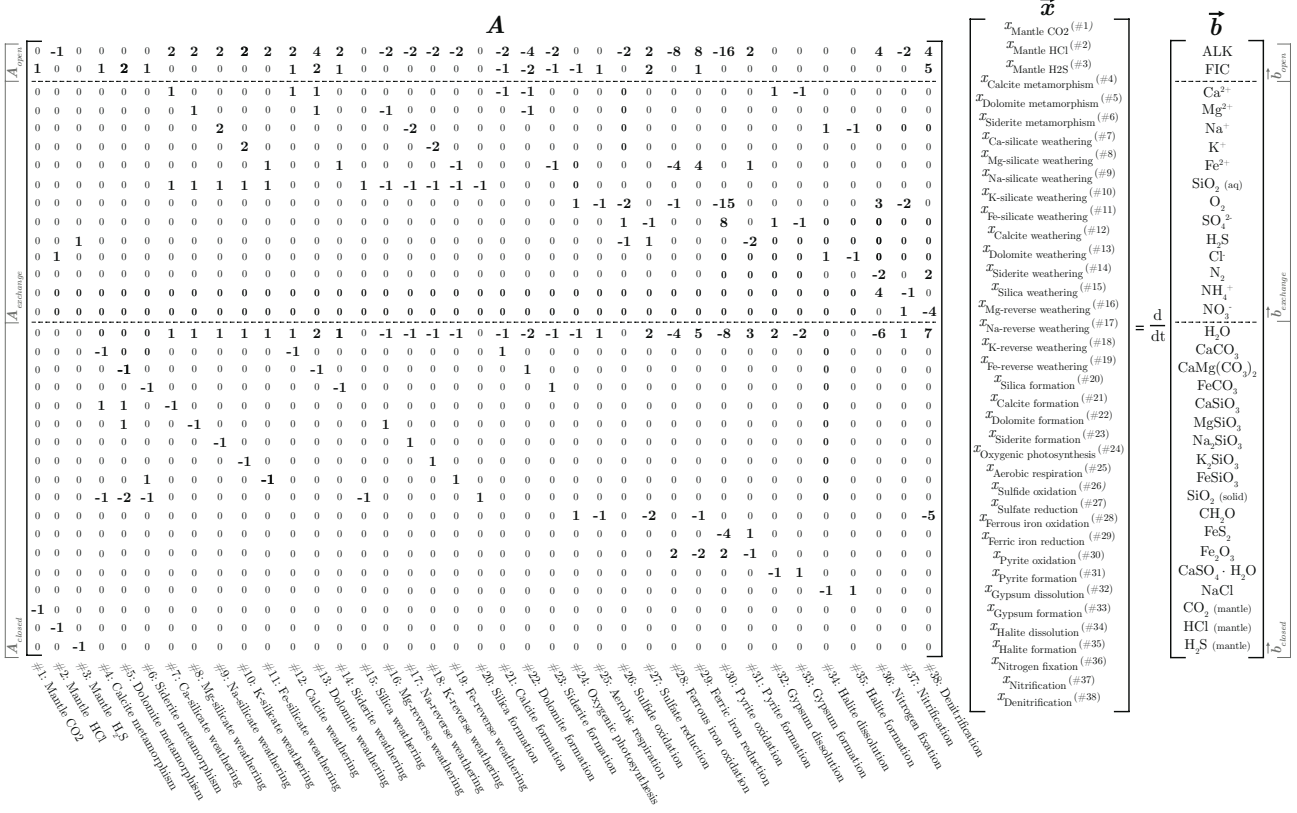

Fig. 1. The equation $\boldsymbol{A}\vec{x} = \vec{b}$ for the biogeochemical processes under consideration (Table 1). Columns of $\boldsymbol{A}$ correspond to reactions and rows correspond to chemical species. Entries in $\boldsymbol{A}$ reflect stoichiometric coefficients (moles/reaction), entries in $\vec{x}$ describe reaction rates (reaction/time), and entries of $\vec{b}$ are time derivatives of chemical species reservoirs (moles/time). Most entries of $\boldsymbol{A}$ are zero as most processes involve only a small number of chemical species. $\boldsymbol{A}_{closed}$ and $\vec{b}_{closed}$ are the entire matrix and vector, $\boldsymbol{A}_{exchange}$ and $\vec{b}_{exchange}$ are resolved only to ocean–atmosphere species (excluding entries for H_2O and lower), and $\boldsymbol{A}_{open}$ and $\vec{b}_{open}$ are resolved only to ALK and FIC (excluding entries for Ca^{2+} and lower).

magnesium, sodium, potassium, and iron silicate phases; dissolution and precipitation of halite and gypsum; and biological cycling of carbon, oxygen, sulfur, nitrogen, and iron. Each process is represented by a simplified chemical reaction that encompasses underlying physical and biochemical steps, and these reactions can be combined to represent net geochemical reaction systems. To establish a convenient reference frame, each chemical species in each reaction is written as its dominant form at the second equivalence point such that the stoichiometric factors on H^+ and CO_2 correspond to fluxes of ALK and fluid inorganic carbon (FIC), where FIC is equal to the sum of pCO_2 and ocean–atmosphere dissolved inorganic carbon (DIC) (32).

Generalizations are made for simplicity; for example, organic matter is presented as a unit carbohydrate without nitrogen, phosphorus, or sulfur, meaning that its oxidation generates FIC but not ALK, while aerobic respiration does not distinguish among environmental settings. Silicate mineral reconstitution is represented with a fixed cation/silica ratio without attempting to capture the range of clay chemistries, the role of aluminum, or environmental context (e.g., high-temperature or low-temperature). We represent sulfur degassing as H_2S in order to capture its likely mantle redox state and speciation; although SO_2 is commonly observed in volcanic systems, that flux could reflect an oxidized product of a reduced precursor. Moreover, because long-term changes in mantle redox state are not directly relevant to evaluating how combinations of biogeochemical processes balance fluxes through the ocean–atmosphere system, as well as due to the long residence time of many chemicals in the mantle, we do not consider subduction fluxes. While many of the reactions in Table 1 may be limited by additional reactants and environmental conditions, such as the availability of nutrients like phosphate, this simplified set of processes best demonstrates how different reaction combinations can result in stable element cycles.

The biogeochemical reactions can be written as a series of differential equations and rearranged into the matrix equation $\boldsymbol{A}\vec{x} = \vec{b}$ (Fig. 1). In this equation, $\boldsymbol{A}$ is an m-by-n matrix of stoichiometric constants (units: moles/reaction), $\vec{x}$ is a vector of length n quantifying reaction rate (units: reaction/time) where all values must be ≥ 0 because each reaction in Table 1 is considered unidirectionally (*SI Appendix*, section S3, *Gross Fluxes and Net Fluxes*), and $\vec{b}$ is a vector of length m describing the time-derivatives of each chemical species (units: moles/time). Under this formalism, a vector $\vec{x}$ of biogeochemical process rates is mapped by matrix $\boldsymbol{A}$ to changes in the size of fluid (dissolved and gaseous) and crustal reservoirs. We consider three forms of $\boldsymbol{A}$ and $\vec{b}$ that each retains all processes but differ in the number of tracked chemical species: $\boldsymbol{A}_{closed}$ and $\vec{b}_{closed}$, $\boldsymbol{A}_{exchange}$ and $\vec{b}_{exchange}$, and $\boldsymbol{A}_{open}$ and $\vec{b}_{open}$. The closed forms include all chemical species, the exchange forms include only dissolved and gaseous chemical species, and the open forms include only ALK and FIC (Fig. 1). Note that we group H_2O with the crustal reservoirs, rather than as a dissolved species, because we are primarily concerned with charged solutes and the modern marine water reservoir is large. Although our analysis includes 38 reactions impacting 33 chemical species, the equations are not linearly independent; the rank of $\boldsymbol{A}_{closed}$, $\boldsymbol{A}_{exchange}$, and $\boldsymbol{A}_{open}$ are only 20, 13, and 2, respectively. By the rank-nullity

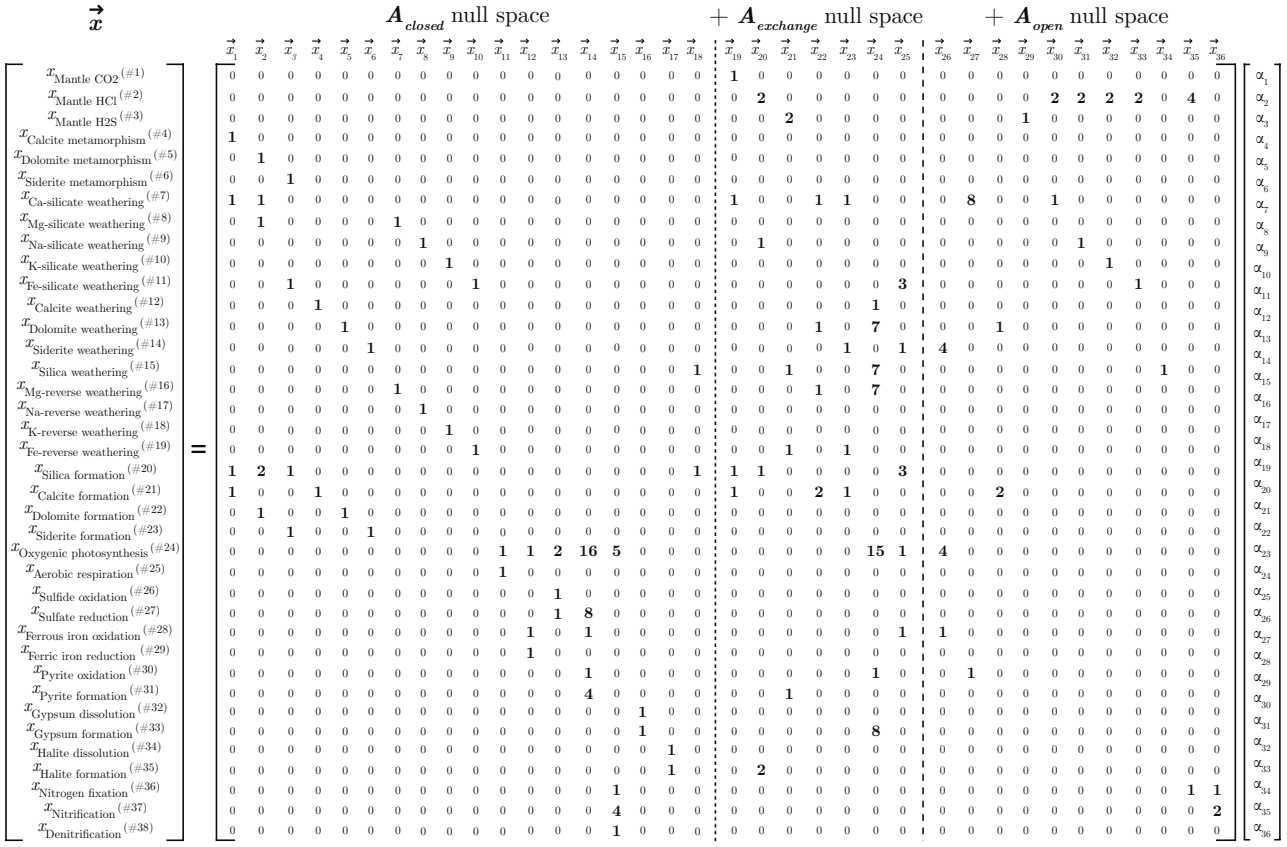

Fig. 2. Basis vectors $(\vec{x}_i)$ for the null space of $\boldsymbol{A_{closed}}$ $(\vec{x}_1 - \vec{x}_{18})$, $\boldsymbol{A_{exchange}}$ $(\vec{x}_1 - \vec{x}_{25})$, and $\boldsymbol{A_{open}}$ $(\vec{x}_1 - \vec{x}_{36})$. Vectors satisfying $\boldsymbol{A}\vec{x} = \vec{0}$ can be expressed as the sum of the relevant basis vectors weighted by α_i values. The α_i values, which reflect the contribution of each basis vector to $\vec{x}$, can be positive or negative as long as each of the values within the final $\vec{x}$ is ≥ 0.

theorem, which relates matrix rank, nullity, and number of matrix columns, the dimensions of the $\boldsymbol{A_{closed}}$, $\boldsymbol{A_{exchange}}$, and $\boldsymbol{A_{open}}$ null spaces are 18, 25, and 36, respectively.

To identify combinations of biogeochemical reactions resulting in steady-state conditions, constant ocean–atmosphere chemistry, or constant ocean–atmosphere ALK and FIC, we calculated the set of vectors in the null spaces of the three different $\boldsymbol{A}$ matrices. Vectors satisfying $\boldsymbol{A_{closed}}\vec{x} = \vec{0}$ are dubbed closed sets and correspond to reaction combinations that generate steady-state conditions by balancing input and output fluxes to all reservoirs. Vectors satisfying $\boldsymbol{A_{exchange}}\vec{x} = \vec{0}$ include the closed sets as well as additional vectors, dubbed exchange sets, and correspond to combinations of biogeochemical reactions that balance fluxes to and from the ocean–atmosphere system but allow for growth or destruction of crustal reservoirs. Vectors satisfying $\boldsymbol{A_{open}}\vec{x} = \vec{0}$ include the closed and exchange sets as well as additional vectors, dubbed open sets, and correspond to reaction combinations that allow ocean–atmosphere chemistry to vary while ALK and FIC fluxes remain balanced. The closed sets, closed + exchange sets, and closed + exchange + open sets thus define 18-, 25-, and 36-dimensional subspaces of $\mathbb{R}^{38}$ corresponding to the null spaces of $\boldsymbol{A_{closed}}$, $\boldsymbol{A_{exchange}}$, and $\boldsymbol{A_{open}}$, respectively (Fig. 2). These three different types of reaction combinations are useful because they capture distinct behaviors through which ALK and FIC fluxes, and thus pCO_2, can remain balanced over different intervals of geological time. Given that the inherent timescale of carbon cycle instability is approximately 1 Myr (2), geochemical conditions over longer timescales can be viewed as quasistatic for the carbon and alkalinity cycles and can thus be described by a combination of closed, exchange, and open sets built from the assumption of balanced ALK and FIC fluxes.

3. Results and Discussion

3.1. Closed Sets: Steady-State Conditions. The first class of $\vec{x}$, closed sets, describes combinations of biogeochemical reactions that result in no change to any chemical reservoirs. We identify 18 such closed sets, $\vec{x}_1$ to $\vec{x}_{18}$, each of which is comprised of two to five mutually canceling biogeochemical reactions (Fig. 3). Because linear combinations of closed sets are also closed sets, the 18 reaction combinations we classify as basis vectors for the null space of $\boldsymbol{A_{closed}}$, although chosen to reflect intuitive biogeochemical combinations (31, 33), are non-unique (*SI Appendix*, section S2, *Derivation of Sets*). The closed sets containing only two reactions entail simple forward and reverse processes, such as the weathering and formation of carbonate minerals, evaporite minerals, and silica; oxygenic photosynthesis and aerobic respiration; or the weathering and reverse weathering of Mg-, Na-, K-, and Fe-silicate (Fig. 3 *B–D*, *G*, and *H*). Closed sets containing three reactions include a sulfur-based set of oxygenic photosynthesis, sulfide oxidation, and microbial sulfate reduction, as well as an iron-based set of oxygenic photosynthesis, ferrous iron oxidation, and reduction of ferric iron (Fig. 3 *D* and *E*). The four-reaction sets include the "Urey" set, comprised of calcite metamorphism, Ca-silicate weathering, calcite formation, and silica formation (33), a siderite-based equivalent to the Urey set, and a nitrogen-based set that balances

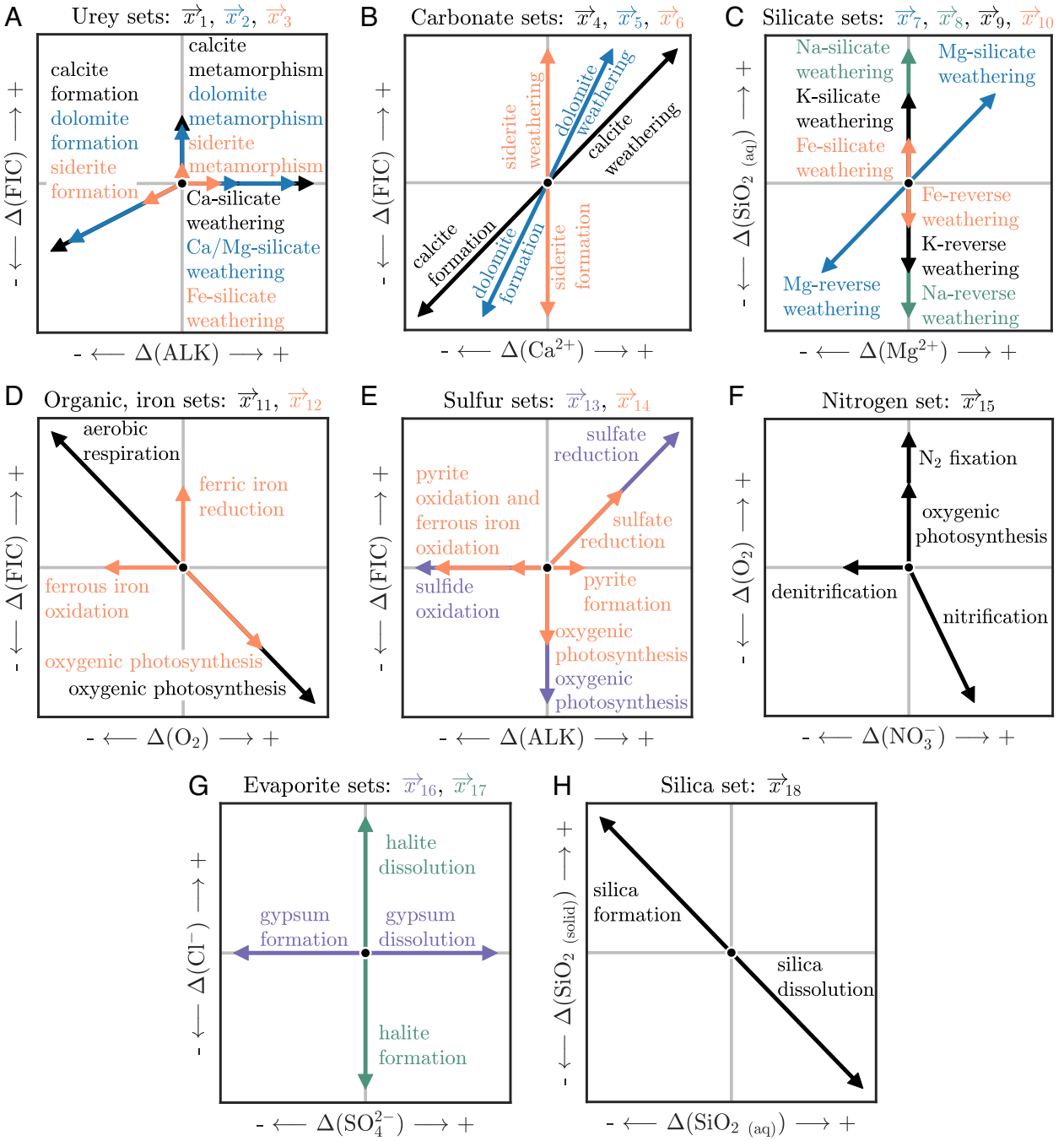

Fig. 3. Closed sets. These mutually canceling combinations of biogeochemical reactions are grouped into categories describing (*A*) Urey-style reactions, (*B*) carbonate weathering and formation, (*C*) silicate weathering and reverse weathering, (*D–F*) cycling of organic matter, iron, sulfur, pyrite, and nitrogen, (*G* and *H*) dissolution and formation of gypsum, halite, and silica. Each closed set can be combined at arbitrary magnitudes with the other closed sets without destabilizing major element cycles. Within each panel, the biogeochemical processes contributing to individual sets are presented in the same color. The plotted scaling for each set is to enhance visibility and does not reflect relative importance in the Earth system.

oxygenic photosynthesis against nitrogen fixation, nitrification, and denitrification (Fig. 3 *A* and *F*). Lastly, the five-process sets include a dolomite version of the Urey set and a pyrite-accommodated version of the sulfur set (Fig. 3 *A* and *E*). Solid-earth degassing processes are not included in the closed sets because we elected not to include reactions describing the return of CO_2, HCl, or H_2S to the mantle through subduction (Table 1), meaning that any amount of solid-Earth degassing would necessitate changing at least one chemical reservoir in the ocean–atmosphere–geosphere system. This choice of reference frame does not impact the utility of our framework as including fluxes into the mantle would not substantially change any of our major conclusions.

The 18 closed sets constrain which biogeochemical reactions must change in concert to maintain steady-state conditions for all reservoirs in the ocean–atmosphere–geosphere system. For example, consider an increase in calcite metamorphism and associated CO_2 degassing, like that commonly proposed during intervals of greater mountain building (34). For all chemical species to attain steady-state conditions following this enhancement, regardless of what those steady-state conditions are, our analysis based on the biogeochemical processes in Table 1 shows that either calcite metamorphism must decrease back to the initial condition or Ca-silicate weathering, calcite formation, and silica formation must all increase; no other combination of reactions can compensate for enhanced

calcite metamorphism without modifying another chemical reservoir. Compensating for increased CO_2 release by increasing organic carbon formation would increase pO_2 or a related reservoir like marine SO_4^{2-}, while decreasing mantle degassing would balance FIC but result in a smaller calcite reservoir and larger Ca-silicate reservoir. Although the reactions within any closed set must increase and decrease together to attain a new steady-state, this framework does not specify either the path(s) to that steady-state or the ultimate steady-state conditions.

Changes to the relative magnitudes of closed sets still yield steady-state conditions. However, within the context of a box model, changes in the magnitudes of closed sets can alter the steady-state conditions even while fluxes among reservoirs remain balanced. This result occurs because steady-state conditions can respond to flux magnitude and not only to the differences between input and output fluxes. Such behavior is analogous to how the steady-state condition for a one-box reservoir with constant input and first-order output depends on the size of the input flux even when inputs and outputs are equal. For example, increases in the strength of the carbonate closed set, consisting of calcite weathering and calcite formation, would increase the delivery of alkalinity to the fluid Earth and deepen the carbonate compensation depth (CCD), altering pCO_2 even while balancing carbonate weathering and formation (15). In general, the dependencies encoded in the equations of numerical models will determine how changes in the magnitude of closed sets manifest as shifts in steady-state conditions.

3.2. Exchange Sets: Constant Ocean–Atmosphere Conditions with Changing Crustal Reservoirs. Evidence from global stratigraphic databases and isotope mass balance models indicates that crustal carbonate, silicate, evaporite, and organic matter reservoirs have gained and lost mass through time even while the climate has remained equable (25, 26, 35). Having established the reaction combinations that fully balance chemical fluxes in the ocean–atmosphere-geosphere system, we thus now turn toward combinations of reactions that can exchange mass among crustal reservoirs while preserving ocean–atmosphere chemistry. We identify 25 such reaction combinations, 18 of which are equivalent to the closed sets and 7 of which are new exchange sets ($\vec{x}_{19}$ to $\vec{x}_{25}$) (Fig. 4). As was the case with closed sets, the seven vectors we classify as new basis vectors for the null space of $\boldsymbol{A_{exchange}}$ are non-unique.

The first three exchange sets account for solid-Earth degassing by converting mantle-derived CO_2 to calcite ($\vec{x}_{19}$), HCl to halite ($\vec{x}_{20}$), and H_2S to pyrite ($\vec{x}_{21}$) (Fig. 4 *A*–*C* and Table 2). These sets enable growth of crustal reservoirs without microbially catalyzed reactions and thus provide mechanisms for accumulating sedimentary deposits during Earth's prebiotic period or on an early warm and wet Mars. Moreover, degassing of CO_2 and carbonate metamorphism are interchangeable for exchange sets because both reactions add exclusively FIC to the ocean–atmosphere system.

The fourth and fifth exchange sets describe the substitution of Ca, Mg, and Fe between carbonate and silicate phases (Fig. 4*D*). Within each of these sets, the transformation of carbonate to silicate

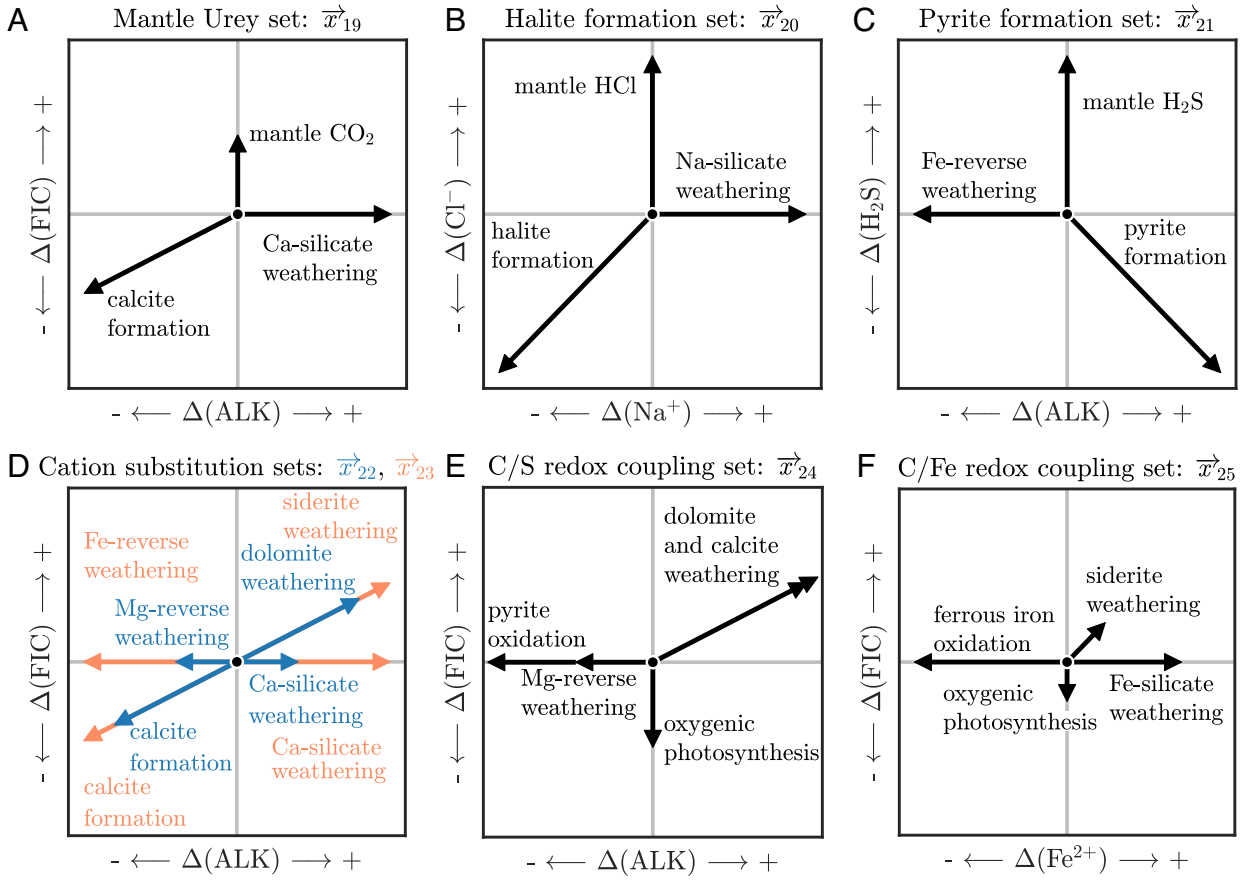

Fig. 4. Exchange sets. These combinations of biogeochemical processes alter the mass of crustal reservoirs without modifying ocean–atmosphere conditions. (*A*–*C*) Exchange sets based around mantle inputs. (*D*) Exchange sets with cation substitution between carbonate and silicate phases. (*E* and *F*) Exchange sets that balance reducing powering by exchanging oxidized carbon and reduced sulfur or iron for reduced carbon and oxidized sulfur or iron. Within each panel, the biogeochemical processes contributing to individual sets are presented in the same color. The plotted scaling for each set is to enhance visibility and does not reflect relative importance in the Earth system. See Table 2 for the chemical reactions associated with each exchange set.

Table 2. Chemical reactions corresponding to exchange sets ($\vec{x}_{19} - \vec{x}_{25}$), notable open sets ($\vec{x}_{26} - \vec{x}_{28}$), and additional exchange and open reactions derived from $\vec{x}_1 - \vec{x}_{36}$ ($\Sigma\vec{x}_i$)

Notes	Reaction
Mantle exchange sets:	
$\vec{x}_{19}$: Mantle Urey	$CO_{2\,(mantle)} + CaSiO_3 \rightarrow CaCO_3 + SiO_{2\,(solid)}$
$\vec{x}_{20}$: Halite formation	$2HCl_{(mantle)} + Na_2SiO_3 \rightarrow 2NaCl + SiO_{2\,(solid)} + H_2O$
$\vec{x}_{21}$: Pyrite formation	$2H_2S_{(mantle)} + Fe_2O_3 + SiO_{2\,(solid)} \rightarrow FeS_2 + FeSiO_3 + 2H_2O$
Cation substitution exchange sets:	
$\vec{x}_{22}$: Ca^{2+}-Mg^{2+} substitution	$CaSiO_3 + CaMg(CO_3)_2 \rightarrow 2CaCO_3 + MgSiO_3$
$\vec{x}_{23}$: Ca^{2+}-Fe^{2+} substitution	$CaSiO_3 + FeCO_3 \rightarrow CaCO_3 + FeSiO_3$
$\Sigma\vec{x}_i$: Fe^{2+}-Mg^{2+} substitution	$FeSiO_3 + CaMg(CO_3)_2 \rightarrow CaCO_3 + FeCO_3 + MgSiO_3$ $\alpha_6 = \alpha_{10} = \alpha_{22} = 1, \alpha_{23} = -1$
Redox balance exchange sets:	
$\vec{x}_{24}$: Redox balance from carbon and sulfur cycles	$4FeS_2 + CaCO_3 + 7CaMg(CO_3)_2 + 7SiO_{2\,(solid)} + 31H_2O \rightarrow 15CH_2O + 8(CaSO_4 \cdot 2H_2O) + 2Fe_2O_3 + 7MgSiO_3$
$\Sigma\vec{x}_i$: Reaction $\vec{x}_{24}$ in reverse	$\alpha_4 = \alpha_{14} = 1, \alpha_5 = \alpha_7 = \alpha_{18} = 7, \alpha_{16} = 8, \alpha_{24} = -1$
$\vec{x}_{25}$: Redox balance from carbon and iron cycles	$3FeSiO_3 + FeCO_3 + H_2O \rightarrow CH_2O + 2Fe_2O_3 + 3SiO_{2\,(solid)}$
$\Sigma\vec{x}_i$: Reaction $\vec{x}_{25}$ in reverse:	$\alpha_6 = \alpha_{12} = 1, \alpha_{10} = \alpha_{18} = 3, \alpha_{25} = -1$
$\Sigma\vec{x}_i$: Redox balance from carbon and iron cycles (alternative)	$4FeSiO_3 + CaMg(CO_3)_2 + H_2O \rightarrow$ $CH_2O + 2Fe_2O_3 + 3SiO_{2\,(solid)} + CaCO_3 + MgSiO_3$ $\alpha_{10} = \alpha_{22} = \alpha_{25} = 1, \alpha_{23} = -1$
$\Sigma\vec{x}_i$: Redox balance from sulfur and iron cycles	$13SiO_{2\,(solid)} + 7Fe_2O_3 + FeS_2 + 2CaSiO_3 + 4H_2O \rightarrow$ $15FeSiO_3 + 2(CaSO_4 \cdot 2H_2O)$ $\alpha_4 = -\frac{1}{4}, \alpha_{10} = \alpha_{18} = \frac{45}{4}, \alpha_{12} = \alpha_{23} = \frac{15}{4}, \alpha_{22} = -\frac{7}{4}, \alpha_{24} = \frac{1}{4}, \alpha_{25} = -\frac{15}{4}$
Select open sets:	
$\vec{x}_{26}$: O_2 from siderite	$4FeCO_3 + 4H_2O \rightarrow 3O_2 + 4CH_2O + 2Fe_2O_3$
$\Sigma\vec{x}_i$: O_2 from siderite (alternative)	$FeCO_3 + H_2O + SiO_{2\,(aq)} \rightarrow O_2 + CH_2O + FeSiO_3$ $\alpha_{10} = \alpha_{18} = 1, \alpha_{25} = -\frac{1}{3}, \alpha_{26} = \frac{1}{3}, \alpha_{34} = -1$
$\Sigma\vec{x}_i$: O_2 from dolomite	$CaMg(CO_3)_2 + H_2O + SiO_{2\,(aq)} \rightarrow O_2 + CH_2O + CaCO_3 + MgSiO_3$ $\alpha_{10} = \alpha_{18} = \alpha_{22} = 1, \alpha_{23} = -1, \alpha_{25} = -\frac{1}{3}, \alpha_{26} = \frac{1}{3}, \alpha_{34} = -1$
$\vec{x}_{27}$: Pyrite oxidation with Ca- silicate weathering	$15O_2 + 4FeS_2 + 8CaSiO_3 \rightarrow 8Ca^{2+} + 8SO_4^{2-} + 2Fe_2O_3 + 8SiO_{2\,(aq)}$
$\vec{x}_{28}$: Carbonate cation switching	$CaMg(CO_3)_2 + Ca^{2+} \rightarrow 2CaCO_3 + Mg^{2+}$

Sets $\vec{x}_{22}$ and $\vec{x}_{24}$ are two of the reservoir exchange reactions of Garrels and Perry (31). Set $\vec{x}_{25}$, from Bachan and Kump (36), is a variant of a reaction from Garrels and Perry (31) with siderite substituted for dolomite (the original reaction is the alternative carbon and iron redox balance). The sulfur and iron redox balance is inspired by Schidlowski et al. (37). Set $\vec{x}_{26}$ is also from Bachan and Kump (36). The closed sets $\vec{x}_1$ to $\vec{x}_{18}$ are not written as reactions because no atoms are net transferred between chemical reservoirs. Chemical reactions for open sets $\vec{x}_{29}$ to $\vec{x}_{36}$ are provided in *SI Appendix*, Eqs. **S85–S92**.

releases FIC while transformation from silicate to carbonate consumes FIC, resulting in no net FIC change (31, 38). For example, $\vec{x}_{22}$ describes the conversion of Ca-silicate and dolomite to calcite and Mg-silicate and $\vec{x}_{23}$ describes the conversion of Ca-silicate and siderite to calcite and Fe-silicate (Table 2). The first reaction, running in the direction of increasing calcite and Mg-silicate at the expense of Ca-silicate and dolomite, has previously been proposed to proceed throughout recent geological time as dolomite was

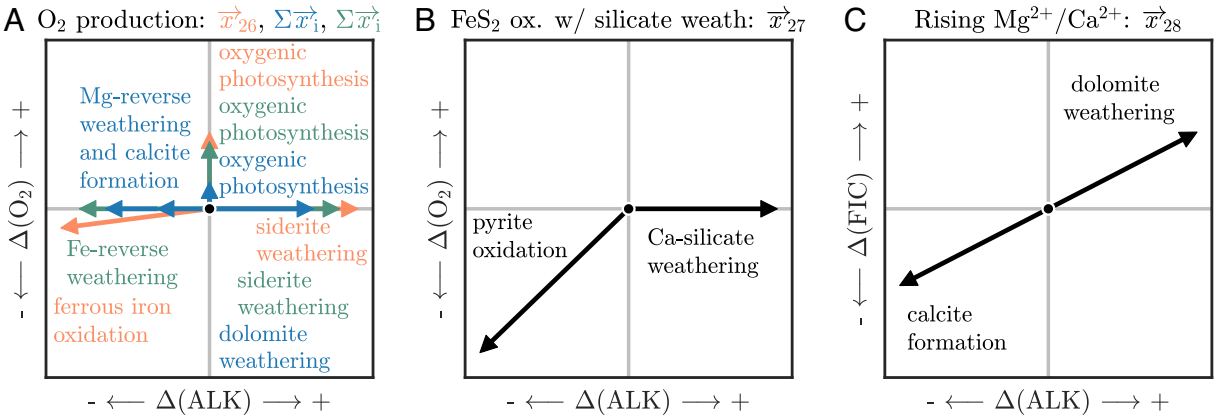

Fig. 5. Open sets that balance ALK and FIC while modifying other ocean–atmosphere chemical species. The biogeochemical processes in (*A*) result in increasing pO_2 (36), those in (*B*) result in declining pO_2 (14), and those in (*C*) result in a rising seawater Mg^{2+}/Ca^{2+} ratio. Note that panel *C* has a different *y*-axis (Δ(FIC)) than panels *A* and *B* (Δ(O_2)). The duration over which open sets can be sustained relates to the strength of reaction feedbacks. Within each panel, the biogeochemical processes contributing to individual sets are presented in the same color. The plotted scaling for each set is to enhance visibility and does not reflect relative importance in the Earth system. See Table 2 and *SI Appendix* for the chemical reactions associated with each open set.

weathered without replacement (27). Overall, these reactions demonstrate that carbonate phases that commonly formed in the past but only rarely today, such as dolomite or siderite, can be converted to calcite and silicate without modifying seawater chemistry or ocean–atmosphere redox state.

The sixth and seventh exchange sets describe the distribution of reducing power among the C, S, and Fe cycles (Fig. 4 *E* and *F*). For example, set $\vec{x}_{24}$ is the well-known reaction of Garrels and Perry (31) describing compensating shifts in the relative abundance of oxidized and reduced carbon and sulfur reservoirs. As pyrite and calcite react to gypsum and organic carbon, reducing power repartitions from the sulfur cycle to the carbon cycle while balancing pO_2 and pCO_2 (25, 26, 39). Set $\vec{x}_{25}$ is a conceptually similar reaction that transfers reducing power between the carbon and iron cycles by converting Fe-silicate and siderite to hematite and organic carbon. Combination of the exchange sets can give rise to a similar reaction balancing Fe-silicate and dolomite against hematite, organic carbon, calcite, and Mg-silicate (31) or to a balance between the sulfur and iron cycles that does not involve any carbon-bearing species (37) (Table 2). Furthermore, closed and exchange sets can be combined to generate additional vectors $\left(\Sigma\vec{x}_i\right)$ with chemical expressions the reverse of those associated with $\vec{x}_{24}$ and $\vec{x}_{25}$.

Although the exchange sets can be combined to generate a wide range of possible reactions, this work demonstrates that there are only a small number of fundamental mechanisms for exchanging mass among crustal reservoirs while preserving constant ocean–atmosphere conditions. Indeed, only four exchange sets ($\vec{x}_{22}$ to $\vec{x}_{25}$) do not rely on inputs from solid-Earth degassing. Although our analysis employs linear algebra to demonstrate this result mathematically, the finding supports the description of reservoir exchange reactions by Garrels and Perry 50 y ago (31).

3.3. Open Sets: Balancing ALK and FIC Fluxes. The final type of $\vec{x}$, open sets, describes reaction combinations that balance ALK and FIC fluxes while allowing for changes in the size of other dissolved, gaseous, and crustal reservoirs. Given that there are 36 linearly independent vectors in the null space of $\boldsymbol{A_{open}}$, there are many ways in which such reaction combinations can occur (*SI Appendix*, Fig. S4). Of the 36 null space dimensions, 25 can be considered as the closed and exchange sets described above while 11 represent new vectors ($\vec{x}_{26} - \vec{x}_{36}$) within the null space of $\boldsymbol{A_{open}}$ (Fig. 2). Once again, these vectors are non-unique. Below, we highlight two types of open sets derived through linear combination of $\vec{x}_1$ through $\vec{x}_{36}$: reaction combinations that accumulate O_2 in the fluid Earth, with relevance to Earth's oxygenation, and reaction combinations that alter seawater chemistry, with relevance to the interpretation of marine geochemical records (Fig. 5).

A key challenge for understanding increases in atmospheric pO_2 is identifying how to balance the budgets of FIC and ALK while substantial quantities of CO_2 are consumed through oxygenic photosynthesis. In prior work, Bachan and Kump (36) argued that oxidation of siderite to hematite could produce three O_2 molecules per four fixed CO_2 molecules (Fig. 5*A*; $\vec{x}_{26}$). Their proposed mechanism is an open set because, by balancing the ALK and FIC fluxes from siderite weathering against ferrous iron oxidation and oxygenic photosynthesis, the reactions preserve ocean–atmosphere ALK and FIC while accumulating O_2. As an extension to this hypothesis, cations bound to carbonate could theoretically also form silicate phases rather than forming oxides. An alternative version of the O_2-generating open set would thus be to convert siderite to Fe-silicate rather than hematite, resulting in 1:1 production of O_2 per fixed CO_2 without modifying ocean–atmosphere ALK or FIC (Table 2). Analogously, dolomite weathering could source CO_2 for conversion to O_2 and, following the formation of Mg-silicate, preserve marine ion chemistry. In this fashion, we observe that reverse weathering, in addition to impacting the major ion chemistry of seawater, may have an under-appreciated role in modulating the production of atmospheric oxygen—the conversion of dolomite and siderite to Mg- and Fe-silicates thus connects O_2 production to the availability of Si and Al for clay formation.

The preceding example balances the positive ALK flux from siderite or dolomite weathering against negative ALK fluxes from iron oxidation, Fe/Mg-reverse weathering, or calcite formation. In a similar way, the positive ALK flux from silicate weathering can be balanced against the negative ALK flux from sulfide oxidation (Table 2), and this open set may be important during periods of enhanced mountain-building (14, 40). For this open set ($\vec{x}_{27}$), atmospheric pO_2 declines while seawater SO_4^{2-} and cation concentrations increase (Fig. 5*B*). However, sulfide oxidation would cease to function as an ALK sink if the atmosphere ran out of O_2 or if the build-up of seawater SO_4^{2-}, given appropriate availability of iron and organic carbon, increased the production of pyrite within sedimentary basins (41, 42). Analogously, reverse weathering during O_2 production, as discussed in the example above, would cease to function as an ALK sink if it were to become limited

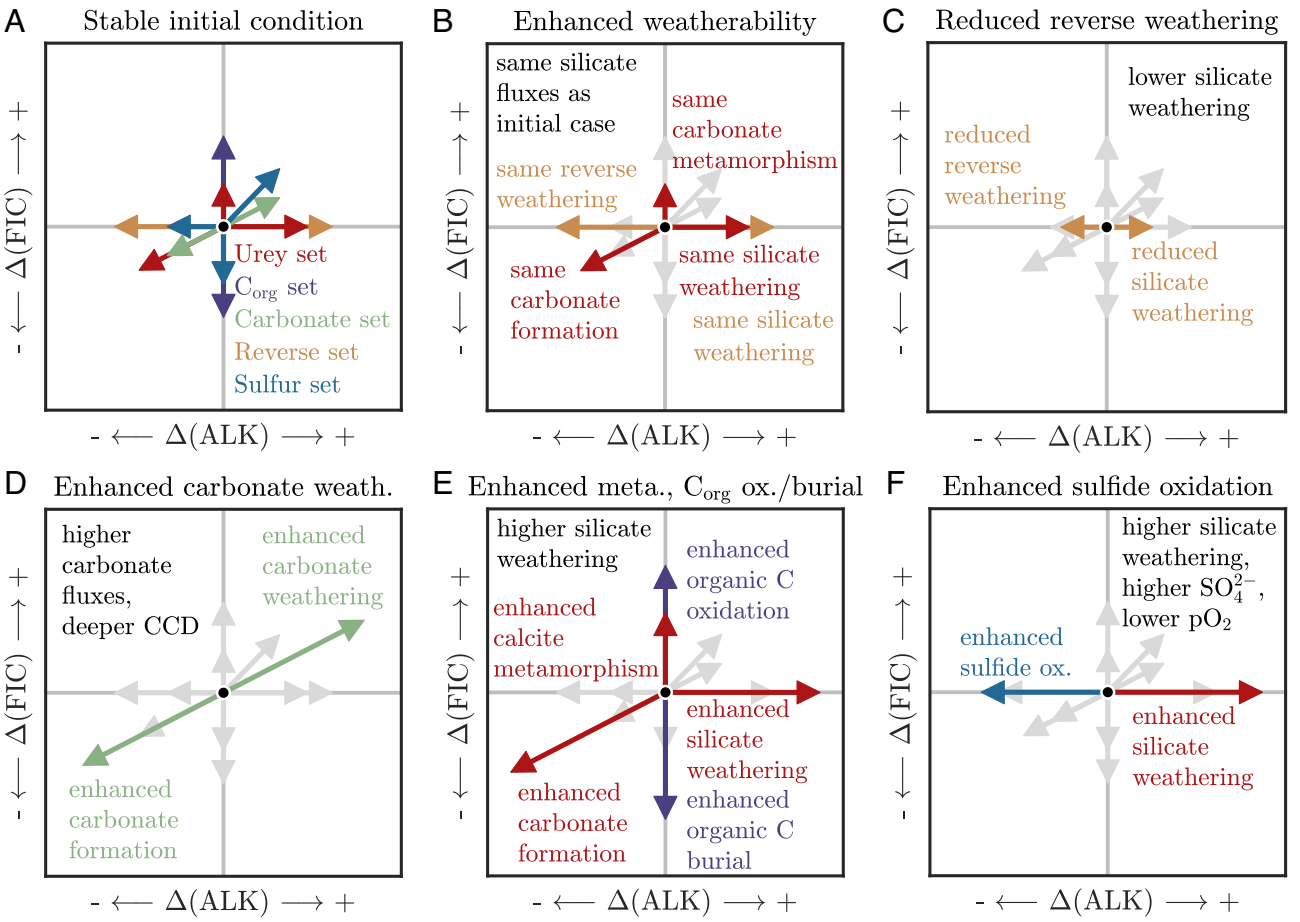

Fig. 6. Hypotheses for Cenozoic climate change as closed and open sets. All arrows in all panels begin at the origin. (*A*) Stable initial condition comprised of the Urey (red), organic carbon (purple), carbonate (green), reverse weathering (yellow), and sulfur (blue) closed sets. (*B*) Constant magnitude of the Urey set or reverse weathering set due to changes in weatherability. (*C*) Reduced magnitude of the reverse weathering set. (*D*) Enhanced magnitude of the carbonate set. (*E*) Enhanced magnitude of the Urey set with enhanced organic carbon oxidation and organic carbon burial. (*F*) Enhanced silicate weathering and oxidation of sulfide minerals. The plotted scaling for each set is to enhance visibility and does not reflect relative importance in the Earth system.

by the availability of reactive Si or Al. Within the context of a box model, the lifetime over which open sets can be sustained thus depends on the functional forms of the feedbacks that couple reactions together.

These examples illustrate the key concept that open sets allow chemical species that can sustain multi-Myr imbalances, such as seawater SO_4^{2-}, to balance the fluxes of ALK and FIC over shorter timescales. When considering long-term planetary evolution, chemical species without stiff reaction feedbacks may thus be critically important for absorbing instabilities in the ALK and FIC cycles over timescales of hundreds of Myr. That is, element cycles capable of accumulating or depleting seawater reservoirs may enable matching between inputs and outputs of ALK and FIC. In an analogous way to SO_4^{2-}, marine ions with long residence times such as sodium and chlorine, although not often considered central players in the global carbon cycle, may actually have key roles in the maintenance of stable pCO_2 values over geological timescales.

4. An Application: Cenozoic Climate Change

The long-term cooling of the Cenozoic and associated decrease in pCO_2 are robust features of geochemical datasets that have been the subject of extensive prior research (43, 44). The drawdown of CO_2 required an imbalance between input and output fluxes of either ALK, FIC, or both. However, as the carbon cycle is thought to be extremely sensitive to sustained imbalances in the fluxes of ALK and FIC (2, 3), understanding the processes that prevented runaway changes in pCO_2 while still allowing for declining Cenozoic values remains central to determining the plausible drivers of climatic change. Here, we recast existing hypotheses for carbon cycle stability during Cenozoic cooling into the framework of closed, exchange, and open sets (Fig. 6). While the hypotheses for Cenozoic climate change make distinct and testable predictions for the magnitude of silicate and carbonate weathering fluxes through time, as well as for the chemical and isotopic evolution of seawater, the framework we present does not currently seek to evaluate the specific contributions of distinct biogeochemical processes to observed geochemical variations.

To clarify the mechanisms of Cenozoic pCO_2 decline, we separately discuss hypotheses that require feedbacks, such as climate-dependent silicate weathering with a weatherability construct, from those that balance biogeochemical fluxes through a shared forcing mechanism. Though our framework purposely does not include feedbacks, they can still be considered in terms of their implications for the magnitudes of closed and open sets. In all cases, variations in biogeochemical processes are evaluated relative to a stable initial state at elevated pCO_2 that reflects operation of the Urey set ($\vec{x}_1/\vec{x}_2/\vec{x}_3$: metamorphism, silicate weathering, carbonate formation), the carbonate set ($\vec{x}_4/\vec{x}_5/\vec{x}_6$: carbonate weathering and formation), the reverse weathering set ($\vec{x}_7/\vec{x}_8/\vec{x}_9/\vec{x}_{10}$: silicate weathering and reverse weathering), the organic carbon set ($\vec{x}_{11}$: aerobic respiration and oxygenic photosynthesis), and the sulfur set

($\vec{x}_{13}$: oxygenic photosynthesis, sulfide oxidation, and microbial sulfate reduction) (Fig. 6*A*).

4.1. Balance in Biogeochemical Cycles: Weatherability and Fluxes with Feedbacks. One of the earliest proposed explanations for decreasing Cenozoic pCO_2 was an increase in planetary weatherability (Fig. 4*B*) (8, 45, 46). Here, we use the term weatherability to refer to the coefficients of a monotonic positive function linking silicate weathering fluxes and pCO_2, recognizing that this simple formulation fails to resolve the nuanced roles of acids, oxidants, and water supply, the dynamics of uplift and soil formation, and the kinetics of weathering reactions. Under the weatherability solution for Cenozoic pCO_2 decrease, the system is still governed by the same closed sets at the same magnitudes as in the initial condition, but the pCO_2 required to generate the requisite alkalinity flux has decreased via a modification of the underlying feedback process. The reduction in pCO_2 is ultimately accomplished through a series of transient, low-magnitude imbalances (8).

A closely related hypothesis for Cenozoic climate change is a reduction in reverse weathering (17). Under this solution, a reduction in the reverse weathering ALK sink causes an excess in the supply of ALK from silicate weathering that, by increasing the ALK concentration of seawater, lowers pCO_2. The imbalance in ALK fluxes is rectified by the silicate weathering feedback, which lowers the ALK supply from silicate weathering. Such coupled changes in silicate cycling constitute a decrease in the magnitude of the reverse weathering closed set (Fig. 6*C*). Depending on the cation identity of the alkalinity, this mechanism could alternatively be an open set that balances ALK and FIC fluxes while resulting in an elevated marine Mg^{2+}/Ca^{2+} ratio (Fig. 5*C*; $\vec{x}_{28}$; Table 2). Notably, while this mechanism for Cenozoic climate change does require a silicate weathering feedback, it does not require a change in weatherability.

A more recent hypothesis, underlain by observations of a deepening CCD and declining Ca^{2+} concentrations, generates Cenozoic cooling by increasing the strength of the carbonate closed set (Fig. 6*D*) (15). In this case, pCO_2 may decline by changing the partitioning of FIC between the ocean and atmosphere following changes in seawater Mg^{2+}/Ca^{2+} and in the size of the marine ALK and FIC reservoirs. This partitioning is sensitive to the magnitude of the carbonate closed set as a result of feedbacks in the cycling of dissolved and solid-phase carbonate in the ocean (47, 48).

While the weatherability hypothesis predicts constant silicate weathering fluxes, the reverse weathering hypothesis predicts decreasing silicate weathering fluxes, and the carbonate hypothesis predicts increasing carbonate weathering fluxes, there are also mechanisms for Cenozoic pCO_2 decline that predict increasing silicate weathering fluxes. Such hypotheses, often motivated by the $^{87}Sr/^{86}Sr$ record, generally rely on additional processes that either add FIC or remove ALK from the ocean–atmosphere system to compensate for enhanced ALK supply. For example, Bickle proposed that the drawdown of CO_2 caused by excess ALK supply from erosion-driven silicate weathering was limited by a related increase in the degassing of CO_2 from carbonate metamorphism (Fig. 6*E*) (49–51). Because this hypothesis enhances metamorphism, silicate weathering, and carbonate formation, it is analogous to increasing the magnitude of the Urey closed set. Under a responsive silicate weathering feedback, this hypothesis would require increased weatherability, in the simplistic sense defined above, in order to result in decreased pCO_2 despite the elevated silicate weathering flux.

In a similar manner to enhanced metamorphic degassing, increases in fossil organic carbon oxidation (Fig. 6*E*) (12, 52) or increases in sulfide mineral oxidation (Fig. 6*F*) (14) tied to increases in mountain uplift could partially compensate for increased silicate weathering and balance the Cenozoic carbon cycle. These mechanisms define open sets because they balance ALK and FIC fluxes while resulting in lower pO_2 and, for the sulfide oxidation scenario, higher seawater SO_4^{2-} concentrations. As in the example of metamorphic decarbonation, these scenarios again require enhanced weatherability to result in decreased pCO_2 when assuming a responsive silicate weathering feedback.

4.2. Imbalance in Biogeochemical Cycles: Fluxes Based on Shared Forcings. The closed and open sets described above reflect changes in Cenozoic pCO_2 governed by the silicate weathering and carbonate compensation feedbacks. In each of these cases, the transient imbalances necessary to decrease pCO_2 over the Cenozoic are sufficiently regulated to avoid runaway changes in climatic conditions. As an alternative to feedback processes, researchers have also proposed that shared forcing mechanisms can limit the magnitude of flux imbalances. In these hypotheses, there is not necessarily a feedback process that keeps input and output fluxes balanced. Rather, a common mechanism such as mountain uplift regulates both sources and sinks such that the net ALK and FIC fluxes are sufficiently small to prevent catastrophic pCO_2 variation. Although feedbacks are commonly employed in numerical models to generate carbon cycle stability (27), compensating fluxes can theoretically also sustain habitable conditions. That is, the processes that act to make silicate weathering fluxes increase, such as enhanced erosion, can also act to elevate pCO_2 by increasing decarbonation reactions or the oxidation of organic carbon and sulfide minerals (14, 49, 52–54). Such mechanisms potentially require a sluggish or absent silicate weathering feedback in order to sustain minor imbalances in ALK and FIC fluxes over the duration of mountain building. Because this type of pCO_2 change is not balanced for ALK and FIC fluxes, such hypotheses are technically outside the conceptual framework presented in this article (Fig. 1). However, as these ideas represent only minor variations from fully balanced systems, their flux diagrams are nearly identical to open and closed sets (Fig. 6 *E* and *F*).

The core mechanism underlying this class of Cenozoic climate change hypotheses is that mountain uplift may increase, in addition to the ALK flux from silicate weathering, metamorphism (49–51), sulfide oxidation (14), organic carbon oxidation (10, 12, 52), or the removal of organic carbon through enhanced sedimentation (9, 55). The net direction of pCO_2 change will depend on the relative erosional enhancement of each process and will likely differ for each orogenic event. For example, pCO_2 could decline without invoking the silicate weathering feedback if an enhancement in silicate weathering exceeded that of sulfide oxidation (Fig. 6*F*) (14). This mode of hypothesis also suggests the potential operation of a closed set composed of tectonically forced organic carbon oxidation and sedimentation-forced organic carbon burial (Fig. 6*E*). Although increasing the magnitude of either organic carbon oxidation or burial may not necessarily induce corresponding change in the other process (56), the two can both be driven by tectonic forcing and thus stably alter pCO_2 through small flux imbalances.

5. Conclusions

This work quantifies interactions among global element cycles using a set of chemical reactions that couple the atmosphere, ocean, and geosphere. We highlight 18 closed sets describing reaction combinations that generate steady-state conditions for all chemical reservoirs and 7 exchange sets that balance fluxes of dissolved and gaseous compounds while accumulating and

depleting crustal reservoirs. Despite considering a wide range of biogeochemical reactions, our analysis reveals that there are only a small number of ways to exchange mass between crustal reservoirs without modifying ocean–atmosphere conditions. We also identify 11 open sets, which are reaction combinations that compensate for imbalances in ALK and FIC fluxes by modifying other chemical reservoirs in the fluid Earth. Because feedbacks determine the timescale over which open sets can be sustained, biogeochemical reactions without stiff feedbacks may be important for the stability of pCO_2 over geological time; the accumulation and depletion of elements in seawater such as SO_4^{2-} and Na^+ may thus have key roles in long-term planetary habitability. Moreover, reverse weathering processes can regulate the transfer of cations from carbonate to silicate phases and may contribute to the accumulation of atmospheric oxygen. Lastly, we demonstrate how existing hypotheses for Cenozoic climate change, based on either assumed climate feedbacks or shared forcing mechanisms, can be viewed in the framework of closed and open sets. This discussion illustrates that different hypotheses make testable predictions for the changes in Cenozoic silicate and carbonate weathering fluxes and highlights the importance of identifying the relative influences of tectonics and climate on biogeochemical processes. Overall, this work provides a systematic conceptual framework for understanding balance and imbalance in global biogeochemical cycles.

6. Method for calculation of sets

The reactions listed in Table 1 were rearranged into Fig. 1 by relating stoichiometric coefficients to reaction rate and impacted chemical species. We then used the MATLAB function *null* with the *rational* option to calculate a non-orthonormal basis for the null spaces of $\boldsymbol{A_{closed}}$, $\boldsymbol{A_{exchange}}$, and $\boldsymbol{A_{open}}$. In turn, we constructed a modified basis for each null space in which each vector was composed of intuitive process combinations with positive magnitudes. While there are an infinite number of possible basis vectors, each reflecting a distinct combination of biogeochemical processes, we reached the basis sets presented here by matching previously described chemical expressions and/or by minimizing the number of biogeochemical processes contributing to each set (*SI Appendix*, Eqs. **S1–S92**).

Data, Materials, and Software Availability. No data were generated for this article. The mathematics that underly our results are solved in a set of MATLAB scripts archived through Zenodo (10.5281/zenodo.10621255) (57) and available on GitHub (github.com/PrestonCosslettKemeny/biogeochemical_sets).

ACKNOWLEDGMENTS. P.C.K. is supported through the TC Chamberlin Fellowship at the University of Chicago and through an NSF EAR postdoctoral fellowship (#2204376). Comments from two anonymous reviewers improved this manuscript.

1. G. L. Foster, D. L. Royer, D. J. Lunt, Future climate forcing potentially without precedent in the last 420 million years. *Nat. Commun.* **8**, 14845 (2017), 10.1038/ncomms14845.
2. R. A. Berner, K. Caldeira, The need for mass balance and feedback in the geochemical carbon cycle. *Geology* **25**, 955–956 (1997).
3. T. T. Isson *et al.*, Evolution of the global carbon cycle and climate regulation on earth. *Global Biogeochem. Cycles* **34**, e2018GB006061 (2020), 10.1029/2018GB006061.
4. J. C. Walker, P. B. Hays, J. F. Kasting, A negative feedback mechanism for the long-term stabilization of Earth's surface temperature. *J. Geophys. Res. Oceans* **86**, 9776–9782 (1981), 10.1029/JC086iC10p09776.
5. S. L. Brantley, A. Shaughnessy, M. I. Lebedeva, V. N. Balashov, How temperature-dependent silicate weathering acts as Earth's geological thermostat. *Science* **379**, 382–389 (2023), 10.1126/science.add292.
6. M. E. Raymo, W. F. Ruddiman, Tectonic forcing of late Cenozoic climate. *Nature* **359**, 117–122 (1992), 10.1038/359117a0.
7. A. J. West, A. Galy, M. Bickle, Tectonic and climatic controls on silicate weathering. *Earth Planet. Sci. Lett.* **235**, 211–228 (2005), 10.1016/j.epsl.2005.03.020.
8. J. K. Rugenstein, A. B. Jost, K. V. Lau, K. Maher, Cenozoic carbon cycle imbalances and a variable weathering feedback. *Earth Planet. Sci. Lett.* **450**, 152–163 (2016), 10.1016/j.epsl.2016.06.035.
9. C. France-Lanord, L. A. Derry, Organic carbon burial forcing of the carbon cycle from Himalayan erosion. *Nature* **390**, 65–67 (1997), 10.1038/36324.
10. R. G. Hilton, J. Gaillardet, D. Calmels, J. L. Birck, Geological respiration of a mountain belt revealed by the trace element rhenium. *Earth Planet. Sci. Lett.* **403**, 27–36 (2014), 10.1016/j.epsl.2014.06.021.
11. V. Galy, B. Peucker-Ehrenbrink, T. Eglinton, Global carbon export from the terrestrial biosphere controlled by erosion. *Nature* **521**, 204–207 (2015), 10.1038/nature14400.
12. J. R. Zondervan *et al.*, Rock organic carbon oxidation CO_2 release offsets silicate weathering sink. *Nature* **623**, 329–333 (2023), 10.1038/s41586-023-06581-9.
13. J. Spence, K. Telmer, The role of sulfur in chemical weathering and atmospheric CO_2 fluxes: Evidence from major ions, $\delta^{13}C_{DIC}$, and $\delta^{34}S_{SO4}$ in rivers of the Canadian Cordillera. *Geochim. Cosmochim. Acta* **69**, 5441–5458 (2005), 10.1016/j.gca.2005.07.011.
14. M. A. Torres, A. J. West, G. Li, Sulphide oxidation and carbonate dissolution as a source of CO_2 over geological timescales. *Nature* **507**, 346–349 (2014), 10.1038/nature13030.
15. L. A. Derry, Carbonate weathering, CO_2 redistribution, and neogene CCD and pCO_2 evolution. *Earth Planet. Sci. Lett.* **597**, 117801 (2022), 10.1016/j.epsl.2022.117801.
16. P. Michalopoulos, R. C. Aller, Rapid clay mineral formation in Amazon delta sediments: Reverse weathering and oceanic elemental cycles. *Science* **270**, 614–617 (1995), 10.1126/science.270.5236.614.
17. A. G. Dunlea, R. W. Murray, D. P. Santiago Ramos, J. A. Higgins, Cenozoic global cooling and increased seawater Mg/Ca via reduced reverse weathering. *Nat. Commun.* **8**, 844 (2017), 10.1038/s41467-017-00853-5.
18. S. Rahman, R. C. Aller, J. K. Cochran, The missing silica sink: Revisiting the marine sedimentary Si cycle using cosmogenic ^{32}Si. *Global Biogeochem. Cycles* **31**, 1559–1578 (2017), 10.1002/2017GB005746.
19. G. Li, H. Elderfield, Evolution of carbon cycle over the past 100 million years. *Geochim. Cosmochim. Acta* **103**, 11–25 (2013), 10.1016/j.gca.2012.10.014.
20. Y. Park *et al.*, Emergence of the Southeast Asian islands as a driver for Neogene cooling. *Proc. Natl. Acad. Sci. U.S.A.* **117**, 25319–25326 (2020), 10.1073/pnas.2011033117.
21. N. M. Bergman, T. M. Lenton, A. J. Watson, COPSE: a new model of biogeochemical cycling over Phanerozoic time. *Am. J. Sci.* **304**, 397–437 (2004), 10.2475/ajs.304.5.397.
22. B. Mills, S. J. Daines, T. M. Lenton, Changing tectonic controls on the long-term carbon cycle from Mesozoic to present. *Geochem. Geophys. Geosyst.* **15**, 4866–4884 (2014), 10.1002/2014GC005530.
23. T. M. Lenton, S. J. Daines, B. J. Mills, COPSE reloaded: An improved model of biogeochemical cycling over Phanerozoic time. *Earth-Sci. Rev.* **178**, 1–28 (2018), 10.1016/j.earscirev.2017.12.004.
24. R. Tostevin, B. J. Mills, Reconciling proxy records and models of Earth's oxygenation during the Neoproterozoic and Palaeozoic. *Interface Focus* **10**, 20190137 (2020), 10.1098/rsfs.2019.0137.
25. R. M. Garrels, A. Lerman, Phanerozoic cycles of sedimentary carbon and sulfur. *Proc. Natl. Acad. Sci. U.S.A.* **78**, 4652–4656 (1981), 10.1073/pnas.78.8.4652.
26. R. M. Garrels, A. Lerman, Coupling of the sedimentary sulfur and carbon cycles: An improved model. *Am. J. Sci.* **284**, 989–1007 (1984), 10.2475/ajs.284.9.989.
27. R. A. Berner, A. C. Lasaga, R. M. Garrels, Carbonate-silicate geochemical cycle and its effect on atmospheric carbon dioxide over the past 100 million years. *Am. J. Sci. (United States)* **283**, (1983), 10.2475/ajs.283.7.641.
28. K. Wallmann, Controls on the Cretaceous and Cenozoic evolution of seawater composition, atmospheric CO_2 and climate. *Geochim. Cosmochim. Acta* **65**, 3005–3025 (2001), 10.1016/S0016-7037(01)00638-X.
29. Y. Donnadieu, Y. Goddéris, G. Ramstein, A. Nédélec, J. Meert, A 'snowball Earth' climate triggered by continental break-up through changes in runoff. *Nature* **428**, 303–306 (2004), 10.1038/nature02408.
30. R. S. Arvidson, F. T. Mackenzie, M. Guidry, MAGic: A Phanerozoic model for the geochemical cycling of major rock-forming components. *Am. J. Sci.* **306**, 135–190 (2006), 10.2475/ajs.306.3.135.
31. R. M. Garrels, E. A. Perry, Cycling of carbon, sulfur, and oxygen through geologic time. *Sea* **5**, 303–336 (1974).
32. R. E. Zeebe, D. Wolf-Gladrow, *CO in Seawater: Equilibrium, Kinetics, Isotopes* (Gulf Professional Publishing, 2001), **vol. 65**.
33. H. C. Urey, On the early chemical history of the earth and the origin of life. *Proc. Natl. Acad. Sci. U.S.A.* **38**, 351–363 (1952), 10.1073/pnas.38.4.351.
34. R. G. Hilton, A. J. West, Mountains, erosion and the carbon cycle. *Nat. Rev. Earth Environ.* **1**, 284–299 (2020), 10.1038/s43017-020-0058-6.
35. S. E. Peters, J. M. Husson, J. Czaplewski, Macrostrat: A platform for geological data integration and deep-time earth crust research. *Geochem. Geophys. Geosyst.* **19**, 1393–1409 (2018), 10.1029/2018GC007467.
36. A. Bachan, L. R. Kump, The rise of oxygen and siderite oxidation during the Lomagundi Event. *Proc. Natl. Acad. Sci. U.S.A.* **112**, 6562–6567 (2015), 10.1073/pnas.1422319112.
37. M. Schidlowski, C. E. Junge, H. Pietrek, Sulfur isotope variations in marine sulfate evaporites and the Phanerozoic oxygen budget. *J. Geophys. Res.* **82**, 2557–2565 (1977), 10.1029/JC082i018p02557.
38. R. M. Garrels, R. A. Berner, "The global carbonate-silicate sedimentary system–Some feedback relations" in *Biomineralization and Biological Metal Accumulation: Biological and Geological Perspectives Papers presented at the Fourth International Symposium on Biomineralization, Renesse, The Netherlands, June 2–5, 1982* (Springer Netherlands, Dordrecht, The Netherlands, 1983), pp. 73–87.
39. C. T. Reinhard, W. W. Fischer, Mechanistic links between the sedimentary redox cycle and marine acid–base chemistry. *Geochem. Geophys. Geosyst.* **20**, 5968–5978 (2019), 10.1029/2019GC008621.
40. D. Calmels, J. Gaillardet, A. Brenot, C. France-Lanord, Sustained sulfide oxidation by physical erosion processes in the Mackenzie River basin: Climatic perspectives. *Geology* **35**, 1003–1006 (2007), 10.1130/G24132A.1.
41. R. A. Berner, Sedimentary pyrite formation. *Am. J. Sci.* **268**, 1–23 (1970), 10.2475/ajs.268.1.1.
42. R. A. Berner, Sedimentary pyrite formation: An update. *Geochim. Cosmochim. Acta* **48**, 605–615 (1984), 10.1016/0016-7037(84)90089-9.
43. J. W. Rae *et al.*, Atmospheric CO_2 over the past 66 million years from marine archives. *Annu. Rev. Earth Planet. Sci.* **49**, 609–641 (2021), 10.1146/annurev-earth-082420-063026.
44. J. Zachos, M. Pagani, L. Sloan, E. Thomas, K. Billups, Trends, rhythms, and aberrations in global climate 65 Ma to present. *Science* **292**, 686–693 (2001), 10.1126/science.1059412.
45. L. R. Kump, M. A. Arthur, "Global chemical erosion during the Cenozoic: Weatherability balances the budgets" in *Tectonic Uplift and Climate Change* (Springer US, Boston, MA, 1997), pp. 399–426.

46. J. K. Rugenstein, D. E. Ibarra, F. von Blanckenburg, Neogene cooling driven by land surface reactivity rather than increased weathering fluxes. *Nature* **571**, 99–102 (2019), 10.1038/s41586-019-1332-y.
47. D. Archer, H. Kheshgi, E. Maier-Reimer, Dynamics of fossil fuel CO_2 neutralization by marine $CaCO_3$. *Global Biogeochem. Cycles* **12**, 259–276 (1998), 10.1029/98GB00744.
48. B. P. Boudreau, J. J. Middelburg, F. J. Meysman, Carbonate compensation dynamics. *Geophys. Res. Lett.* **37**, L03603 (2010), 10.1029/2009GL041847.
49. M. J. Bickle, Metamorphic decarbonation, silicate weathering and the long-term carbon cycle. *Terra Nova* **8**, 270–276 (1996), 10.1111/j.1365-3121.1996.tb00756.x.
50. D. M. Kerrick, K. Caldeira, Paleoatmospheric consequences of CO_2 released during early Cenozoic regional metamorphism in the Tethyan orogen. *Chem. Geol.* **108**, 201–230 (1993), 10.1016/0009-2541(93)90325-D.
51. D. M. Kerrick, K. Caldeira, Metamorphic CO_2 degassing from orogenic belts. *Chem. Geol.* **145**, 213–232 (1998), 10.1016/S0009-2541(97)00144-7.
52. R. A. Beck, D. W. Burbank, W. J. Sercombe, T. L. Olson, A. M. Khan, Organic carbon exhumation and global warming during the early Himalayan collision. *Geology* 23, 387–390 (1995).
53. J. M. Edmond, Y. Huh, "Chemical weathering yields from basement and orogenic terrains in hot and cold climates" in *Tectonic Uplift and Climate Change* (Springer US, Boston, MA, 1997), pp. 329–351.
54. C. S. Riebe, J. W. Kirchner, D. E. Granger, R. C. Finkel, Strong tectonic and weak climatic control of long-term chemical weathering rates. *Geology* **29**, 511–514 (2001).
55. R. A. Berner, D. E. Canfield, A new model for atmospheric oxygen over Phanerozoic time. *Am. J. Sci.* **289**, 333–361 (1989), 10.2475/ajs.289.4.333.
56. H. E. Hartnett, R. G. Keil, J. I. Hedges, A. H. Devol, Influence of oxygen exposure time on organic carbon preservation in continental margin sediments. *Nature* **391**, 572–575 (1998), 10.1038/35351.
57. P. C. Kemeny, PrestonCosslettKemeny/biogeochemical_sets: SetsCode_v1, February 5, 2024 release [Software]. Zenodo (2024).